Philosophical Magazine,
Vol. 85, No. 20, 11 July 2005, 2197–2210

Taylor & Francis
Taylor & Francis Group

Low-temperature solubility of copper in iron: experimental study using thermoelectric power, small angle X-ray scattering and tomographic atom probe

M. PEREZ*†, F. PERRARD‡[1], V. MASSARDIER†, X. KLEBER†, A. DESCHAMPS‡, H. DE MONESTROL§, P. PAREIGE§ and G. COVAREL†

†GEMPPM, UMR CNRS 5512, Institut National des Sciences Appliquées de Lyon, 69621 Villeurbanne Cedex, France
‡LTPCM, CNRS UMR 5614, Institut National Polytechnique de Grenoble, Domaine Universitaire, BP 75, 38 402 St Martin d'Hères Cedex, France
§GPM, CNRS UMR 6634 Université de Rouen, Avenue de l'université, BP 12, 76801 Saint Etienne du Rouvray, France

(*Received 1 December 2004; in final form 4 February 2005*)

Measuring the solubility limit of copper in iron at temperature lower than 700°C is problematic because copper diffusion is too slow in this temperature range. To overcome this difficulty, fine precipitation of copper is studied. The solubility limit of copper is measured after complete precipitation using two complementary techniques: thermoelectric power and small angle X-ray scattering. Values obtained are confirmed by tomographic atom probe and give results much higher than what is usually extrapolated from high-temperature experiments.

1. Introduction

Binary iron–copper alloys have been extensively studied in the last fifty years because copper is a very good candidate for structural hardening of many industrial iron-based alloys like transformation-induced plasticity (TRIP) steels [1], high-strength low alloy (HSLA) steels [2], reactor pressure vessel steels [3, 4] and many other high-performance steels (see the review of Llewellyn on the adverse and the beneficial effects of copper in a wide range of commercial steels [5]). This is due to the fact that copper induces: (i) grain refinement by lowering the $\alpha \leftrightarrow \gamma$ transformation temperature and (ii) precipitation hardening after rapid cooling and tempering. See the paper by Charleux *et al*. [6] for the description of precipitation hardening mechanism. In particular, the presence of 1.5% of copper in steel can lead to an increase in yield strength of 230 MPa. In order to identify the precipitates responsible for this hardening, the precipitation sequence of the binary iron–copper system has been extensively characterized, mostly using transmission electron microscopy

*Corresponding author. Email: michel.perez@insa-lyon.fr
[1]Present address: Arcelor Research, Maizières lès Metz, France.

Philosophical Magazine
ISSN 1478–6435 print/ISSN 1478–6443 online
http://www.tandf.co.uk/journals
DOI: 10.1080/14786430500079645

(TEM) [7] and extended X-ray absorption fine structure (EXAFS) [8]. It has been shown that precipitation begins with the formation of spherical clusters having a metastable bcc structure coherent with the iron matrix. When these clusters reach a critical size (characterized by a diameter of the order of 4 to 6 nm), they transform to the equilibrium fcc structure and become incoherent. According to Othen *et al.* [7], an intermediate 9R precipitate exists, leading to the overall precipitation sequence:

$$\text{solid solution} \rightarrow \text{bcc} \rightarrow \text{9R} \rightarrow \text{fcc}.$$

Despite this relative complexity of the precipitation sequence, the binary iron–copper system is quite often used as a model alloy to validate precipitation models [9–14], due to the spherical nature of precipitates, and to the fact that copper precipitates are reported to be pure copper even in the earlier stages of formation.

In all cases, the knowledge of the thermodynamics of this system, namely the solubility limit and diffusion coefficient, is essential. Such properties have been precisely measured by macroscopic techniques like diffusion couples [15]. These techniques involve long-range diffusion and are therefore limited to temperatures higher than 700°C. Unfortunately, copper precipitation in steels is technologically relevant at temperatures ranging from 550 to 600°C. For this temperature range, the copper solubility is generally extrapolated from high-temperature results, which may lead to important discrepancies. Moreover such extrapolation has been proven wrong [16], which is not surprising due to the complex nature of iron in this temperature range (para-ferromagnetic transition).

In this paper, we employ an experimental approach combining different techniques, namely thermoelectric power (TEP), tomographic atom probe (TAP) and small angle X-ray scattering (SAXS) to determine the solubility limit of copper in pure iron at temperatures ranging from 500 to 700°C. These techniques are used to follow the precipitation kinetics of copper in iron from the supersaturated solid solution. In the investigated temperature range, diffusion is limited to a very small scale. At this scale, attention has to be focused on surface phenomena like the Gibbs–Thomson effect [17]: the interfacial energy of the precipitates is no longer negligible compared to their Gibbs energy, leading to an increase of the solute solubility. Among all the techniques used in the present work, TEP and TAP give access to the copper content in solid solution in iron (TEP giving a mean value and TAP a local measurement), whereas SAXS is expected to evaluate precipitates radii and to give therefore an estimation of the amplitude of the Gibbs–Thomson effect.

In the next section, TEP, TAP, SAXS and the model alloy used for the study will be presented. Then, results from the three techniques will be compared leading to the validation of the approach. Lastly, a discussion relative to the precipitation kinetics and the solubility limit of copper in iron will be held.

2. Materials and experimental techniques

2.1. *Materials*

The model alloy used in this study is a pure binary iron–copper alloy with 1.4 wt% copper, for which all other elements are present at a content lower than 5 ppm. It has

Table 1. Chemical composition of the model alloys used in this work.

Alloy	Cu (wt%)	C (ppm)	S (ppm)	O (ppm)	N (ppm)
Fe–1.4% Cu	1.40	4	1	6	1
Fe–0.8% Cu	0.79	100	50	–	180
Fe	–	2	1	4	2

been processed by the PECM laboratory of the Ecole des Mines de Saint-Etienne (lecoze@emse.fr). Copper and iron were melted together, rolled down to a 1 mm thickness, homogenized in a vacuum furnace and quenched in cold water. The chemical composition of the alloy was determined (see table 1). A full solid solution of copper was obtained by a solution treatment of 30 min at 850°C followed by a water quench, leading to a fully equiaxed ferritic structure with a grain size of approximately 10 μm. Ageing treatments were conducted from 450 to 700°C in salt baths for all *ex situ* experiments. In order to calibrate the TEP measurements, another binary (Fe–0.8wt% Cu) model alloy and a pure iron sample have also been studied. Their compositions are given in table 1.

2.2. *Thermoelectric power*

Characterization of the evolution of the solute content during precipitation in the Fe–1.4 wt% Cu alloy was achieved using thermoelectric power measurements (TEP). The principle of TEP measurements [18] is to establish a temperature gradient (ΔT) at the junctions of the studied alloy with two blocks of pure metal (here, pure iron) and to measure the voltage (ΔV) arising from the Seebeck effect between the two junctions. For the apparatus used in this work, the temperature of the blocks is T and $T+\Delta T$ with $T=15$°C and $\Delta T=10$°C and the relative TEP (denoted S) of the alloy with respect to the TEP of pure iron is given at room temperature in μV/K. This relative TEP is defined as follows:

$$S = S^* - S_0^* = \frac{\Delta V}{\Delta T}, \tag{1}$$

where S^* is the TEP of the alloy and S_0^* is that of pure iron.

The value of S is affected by the defects present in the lattice of the iron matrix and can be considered as being the sum of various contributions: $S=\Delta S_{ss}+\Delta S_d+\Delta S_{pre}$, where ΔS_{SS}, ΔS_d and ΔS_{pre} are due to the elements in Solid Solution (SS), to the dislocations (d) and to the precipitates (pre).

The contribution of the elements in solid solution on the TEP of pure iron is given by the Gorter–Nordheim law [19]. When copper is the only element in solution with a copper content [Cu] expressed in wt%, this law can be written as follows:

$$\Delta S_{SS} = \frac{\alpha_{Cu} S_{Cu} [Cu]_{wt\%}}{\rho_{alloy}} = \frac{\alpha_{Cu} S_{Cu} [Cu]_{wt\%}}{\rho_0 + \alpha_{Cu} [Cu]_{wt\%}}, \tag{2}$$

or equivalently, as follows:

$$\frac{1}{\Delta S_{SS}} = \frac{A}{[Cu]_{wt\%}} + B \quad \text{with} \quad A = \frac{\rho_0}{\alpha_{Cu} S_{Cu}} \quad \text{and} \quad B = \frac{1}{S_{Cu}}. \tag{3}$$

In relation (2), α_{Cu} and S_{Cu} are the specific resistivity and the specific thermoelectric power of copper in solution in pure iron; ρ_0 is the resistivity of pure iron (i.e. $9.9\,\mu\Omega\,cm$) and ρ_{alloy} is that of the studied alloy (which is given by the Matthiessen's rule). Relation (3) shows that the experimental plot of $1/\Delta S_{SS}$ as a function of $[Cu]^{-1}$ is assumed to be linear if the Gorter–Nordheim law is satisfied and can lead to the evaluation of the constants A and B of relation (3). As far as the dislocations are concerned, they tend to decrease the TEP of pure iron and lead to a TEP variation which is related to the dislocation density.

Lastly, the precipitates have an effect on the TEP if they are small and coherent. This effect, though well established experimentally, is not completely understood. Different studies [20, 21] have shown that this effect depends on the type, size, morphology and volume fraction of the precipitates. According to [21], the sign and amplitude of the effect can be reasonably well rationalized in terms of Bragg scattering by coherent precipitates. In the case where the precipitates are coarse and incoherent, it has always been observed that they have no effect on the TEP. As a consequence, during the formation of such precipitates, the measured TEP variations are essentially linked to the decrease in the solute content in solid solution.

Referring to the preceding considerations, it seems possible to follow the copper precipitation in the studied alloy during isothermal treatments through TEP measurements. In the present work, in order to follow the copper precipitation, the relative TEP of the alloy, noted S_t, was measured after different treatment times at the considered ageing temperature and the precipitation kinetics were characterized by the change of S_t as a function of time. The evolution of S_t during the precipitation is assumed to be the result of two main effects: one due to the decrease in the copper content in solution (ΔS_{SS}) and one due to the precipitates themselves if they are small and coherent (ΔS_{pre}). At the end of the precipitation, the precipitates are coarse and incoherent and are thus such that $\Delta S_{pre} = 0$. As a consequence, the TEP value of the alloy obtained at the end of the precipitation, $S_{t\to\infty}$, depends only on the copper content in solution and is thus equal to ΔS_{SS}. This value of $S_{t\to\infty}$ ($=\Delta S_{SS}$) obtained at each temperature can then be converted into the solubility limit of copper in iron using relation (3). However, this determination necessitates a preliminary work aimed at determining the constants A and B of relation (3).

2.3. *Small-angle X-ray scattering*

Small-angle X-ray scattering (SAXS) is a powerful technique for the study of precipitation kinetics in metals. The characterization of the Fe–Cu system is somewhat difficult because of the poor contrast between Fe and Cu atoms. However, this problem can be overcome with synchrotron X-ray sources using the anomalous effect [10]: the accurate selection of an energy close to the Fe edge maximizes the contrast between precipitates and matrix while limiting the fluorescence of Fe.

These experiments were performed on the D2AM beam line at European Synchrotron Radiation Facility (ESRF) in Grenoble. A wavelength λ of 1.7449 Å ($E = 7.106$ KeV) was chosen, leading to a contrast eight times greater compared to a non-anomalous scattering situation.

The optimal sample thickness was obtained after mechanical grinding down to 50 μm and then electropolishing down to 20–30 μm with a 5% perchloric acid–95% acetic acid solution at 15°C and a polishing voltage of 25 V.

The scattering signal was recorded using a two-dimensional CCD camera located at a controlled distance from the sample in order to access to a selected scattering vector (q) range. For a distribution of spherical precipitates, volume fraction (f_v) can be deduced from the relation between the invariant Q_0 (area under the curve in the $Iq^2 = f(q)$ plot), the scattered intensity I and the contrast $\Delta\rho$ [22]:

$$Q_0 = \int_0^\infty I(q)q^2 \, \mathrm{d}r = 2\pi^2(\Delta\rho)^2 f_v(1 - f_v). \tag{4}$$

The absolute volume fraction could then be obtained using a calibrated polyethylene (Lupolen [23]) sample, which would lead to uncertainties of about ±15%. In order to remove this discrepancy and for comparative purposes with TEP kinetics, volume fractions obtained by SAXS have been changed to relative transformed fractions [12]: all SAXS volume fractions have been divided by the final value obtained at the studied temperature.

The precipitate radius can also be deduced from these experiments, using the Guinier approximation:

$$I(q) \propto \exp\left(-\frac{q^2 R_g^2}{3}\right), \tag{5}$$

where R_g is the Guinier radius. This radius can be converted into an absolute value using a simulation of the scattering behaviour by a distribution of copper precipitates in the matrix [24].

Most of the experiments were carried out *in situ* under the X-ray beam with a resistance furnace (up to 10°C/s heating rate). Longer ageing times at 500°C have been carried out *ex situ* in order to limit the length of experiments. Counting rates enabled a measuring time below 10 s.

2.4. *Tomographic atom probe*

Tomographic atom probe (TAP) characterization of the Fe–1.4wt% Cu alloy annealed at 500°C was performed with the GPM TAP [25]. TAP is the only analytical technique that has sufficient spatial resolution to distinguish between copper in solid solution and copper in clusters or precipitates [26]. TAP specimens were electropolished using standard procedures [27] from blanks that were cut from aged materials described in Section 2.1.

The experimental conditions required to obtain accurate TAP data are well known for these ferritic steels. In particular, it is necessary to cool the specimen to a temperature of 50 K to avoid a systematic error on the copper level measurement. A pulse fraction of 19% and a pulse repetition rate of 1700 Hz were used. Most of the analysed volumes contained contributions of copper-enriched clusters or

precipitates. In order to have an accurate measurement of the copper level in solid solution ([Cu]) and in order to avoid the possibility of solute tails or depleted zone from biasing the data, the matrix region surrounding the precipitates has been excluded from the data files. Concentration uncertainties (2σ) due to counting statistics are given by the standard deviation $2\sigma = 2\sqrt{([Cu]_{at.\%}(1-[Cu]_{at.\%})/N)}$ where $[Cu]_{at.\%}$ is the atomic copper concentration in the matrix.

3. Results and discussion

3.1. *Precipitation kinetics followed by TEP*

3.1.1. Validation of the Gorter–Nordheim law and calibration of the TEP measurements. Before using TEP to assess the solubility limit of copper in iron, it was necessary to check the validity of the Gorter–Nordheim law in the case of the iron–copper system and to determine the coefficients A and B of relation (3). To this end, the relative TEP (S) of the Fe–0.8 wt% Cu alloy and that of the Fe–1.4 wt% Cu alloy were measured after complete solubilization of copper at high temperature and water-quench. Moreover, the resistivity of the alloys was assessed, knowing that it can be calculated from the empirical relation of Meyzaud *et al.* [28] giving the resistivity of a steel at room temperature as a function of the content of its alloying elements in solution expressed in wt%. In the case of the studied alloys, this relation can be written as follows:

$$\rho_{alloy}(\mu\Omega cm) = 9.9 + \alpha_{Cu}[Cu]_{wt\%} \quad \text{with} \quad \alpha_{Cu} = 3.9\left(\frac{\mu\Omega\,cm}{wt\%}\right). \tag{6}$$

In this approach, the effects of other alloying elements such as C, S, O, N on the TEP and on the resistivity were considered to be negligible. This is all the more reasonable as the concentration of these elements is very low compared to that of copper.

The evolution of the product between the resistivity and the relative TEP ($\rho_{alloy}\,S$) could then be plotted as a function of the copper content in solution (figure 1). As can be seen in figure 1, this evolution is linear. This result is in good agreement with the Gorter–Nordheim law expressed in the form of relation (2) which predicts that the slope of the evolution is equal to the product between α_{Cu} and S_{Cu}. As a consequence, from the slope of the straight line of and from the knowledge of the value of α_{Cu}, the specific TEP of copper in iron, S_{Cu}, could be assessed: $S_{Cu} = -(23.4 \pm 0.5)$ $\mu V/K$. This specific TEP is negative. This indicates that: (i) copper atoms in solution in iron decrease the TEP of iron and (ii) a decrease in the copper content in solution (due to a precipitation phenomenon) is expected to lead to a TEP increase.

From the evaluation of S_{Cu}, the constants A and B of relation (3) were calculated and relation (3) was written in the following manner:

$$\frac{1}{\Delta S_{SS}}\ (\mu V/K)^{-1} = -\frac{0.1086}{[Cu]_{wt\%}} - 0.04276. \tag{7}$$

It has to be pointed out that this relation is in good agreement with the values of S measured on the two Fe–Cu alloys after complete solubilization of copper and

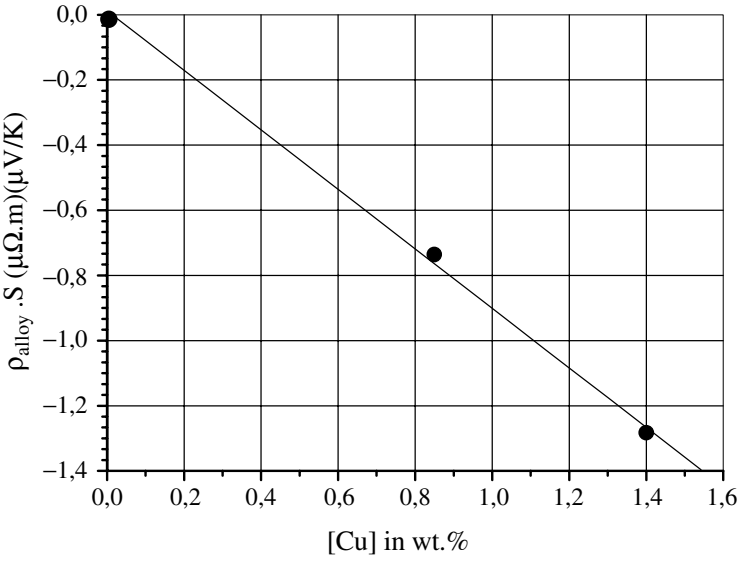

Figure 1. Product of the TEP by the resistivity as a function of the copper content for pure iron and two binary Fe–Cu alloys. These measurements are in good agreement with the Gorter–Nordheim relation.

water-quench. Furthermore, relation (7) makes possible the evaluation of the solubility limit of copper in iron, from the TEP values ($S_{t\to\infty}$) obtained at the end of the precipitation at each temperature, as explained in Section 2.2.

3.1.2. Analysis of the TEP kinetics obtained on the Fe–1.4 wt% Cu alloy. In figure 2, TEP evolution during ageing at 500°C is compared with Vickers hardness measurements. After an initial increase of hardness (associated with the nucleation and growth of the precipitates), the hardness passes through a maximum and then decreases due to the growth and coarsening of the precipitates. At the same time, the TEP gradually increases according to a sigmoidal evolution before stabilizing. This TEP evolution can thus be attributed to precipitation of copper.

Figure 3 shows the evolution of the TEP for different ageing temperatures ranging from 450 to 700°C. Experimental data exhibit very low scattering giving confidence into the technique and its accuracy. For ageing temperatures higher than 500°C, kinetics have been followed until the end of precipitation characterized by a stabilization of TEP at a final value which depends on the ageing temperature. For lower ageing temperatures, the end of the precipitation kinetics has not been reached because the corresponding ageing time was too long.

Three important points can be deduced from these evolutions: (i) the sigmoidal evolution of the TEP curves tells us how fast precipitation occurs: it can be seen that increasing the temperature accelerates the precipitation until 575°C (above this temperature, the precipitation is slowed down by increasing the temperature (typical 'C' curve)); (ii) the final TEP level is directly linked to the solubility limit of copper in iron; (iii) precipitate volume fractions can be directly calculated using relation (7),

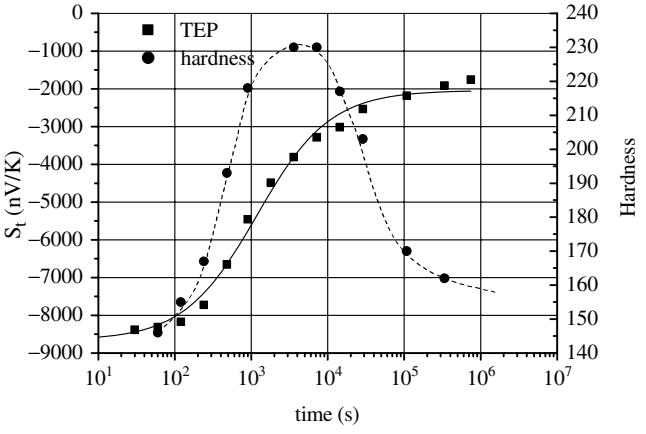

Figure 2. Evolution of the TEP and of the Vickers hardness during an isothermal ageing performed at 500°C. The sigmoidal evolution of the TEP kinetic can be attributed to the copper precipitation.

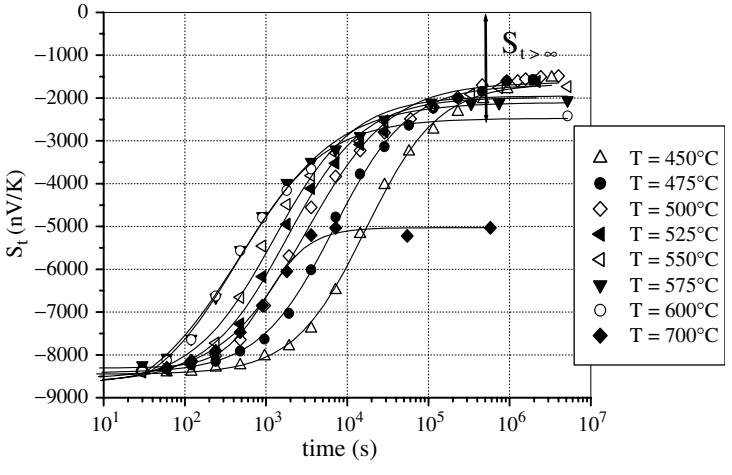

Figure 3. Evolution of the TEP as a function of time after solubilization, water-quench and ageing of the Fe−1.4 wt%Cu alloy at different temperatures. These measurements allow the precipitation kinetics to be characterized and the solubility limit of copper in iron to be assessed.

subtracting the amount of copper in solid solution at a given time, from its initial value (1.4 wt%), and introducing the density of copper precipitates.

3.2. *Precipitate radii and transformed fraction (SAXS and TEP)*

The evolution of precipitate mean radii versus time for three temperatures is presented in figure 4. This plot demonstrates the coarsening behaviour of this system

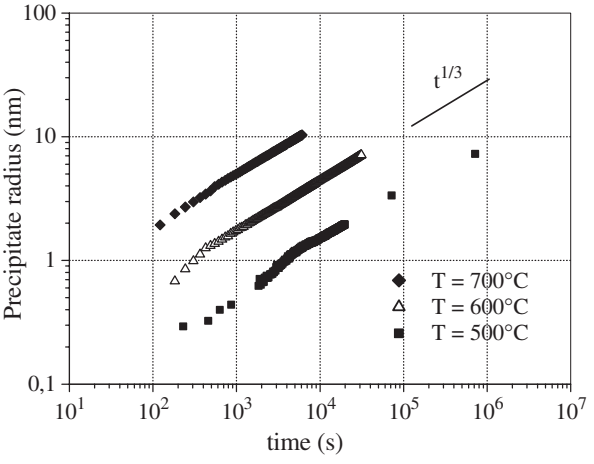

Figure 4. *In situ* evolution of radii during ageing at three different temperatures. The coarsening stage ($R \propto t^{1/3}$) is well defined for long ageing times.

for long ageing times. Indeed, according to the LSW theory, coarsening (or Ostwald ripening) takes place when precipitation reaction is complete and is characterized by growth of precipitates bigger than the mean radius and dissolution of smaller ones, the precipitated volume fraction being almost constant. The growth law of the mean radius in the coarsening regime is of the form: $R \propto t^{1/3}$ [29, 30]. We can see that our results are in very good agreement with this theory, as reported before by Monzen *et al*. [31]. They could therefore be reasonably extrapolated for longer ageing times.

The relatively large radii (greater than 6 nm) measured or extrapolated from SAXS measurements at longer ageing times (10^6 s), give us good confidence in the measurement of the solubility limit that will be performed at these times. Indeed, precipitates larger than 6 nm are considered to be in their equilibrium fcc and incoherent structure. As a consequence, they will have no influence on TEP measurements (see Section 2.2).

Transformed fraction is defined by the ratio of precipitate volume fraction at a given time over precipitate volume fraction at infinite time: it ranges from 0 (no precipitation) to 1 (fully precipitated state). Transformed fraction deduced from TEP is compared with normalized *in situ* and *ex situ* SAXS measurements at 500 and 600°C in figure 5. This comparison shows that at both temperatures, the agreement between the two techniques is remarkably good. Both techniques give access to the kinetics of precipitation at any temperature. However, TEP measurements, which are easier to implement, should be performed preferentially to follow the evolution of transformed fraction as well as the copper content in the solid solution during copper precipitation in ferrite.

TEP results, in terms of transformed volume fraction should be considered with caution in the very first stages of precipitation. Indeed, when precipitates are small, i.e. when they are coherent, and thus mechanically perturbing the surrounding matrix, TEP is affected by the precipitates themselves, which is contradictory with our assumption that only the copper content affect the TEP measurement.

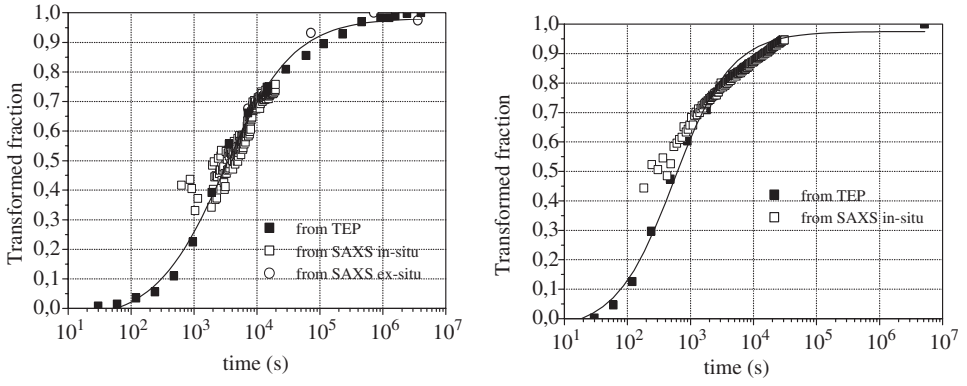

Figure 5. Transformed fraction evolution during ageing at 500°C (left) and 600°C (right). TEP and SAXS measurements are in remarkably good agreement.

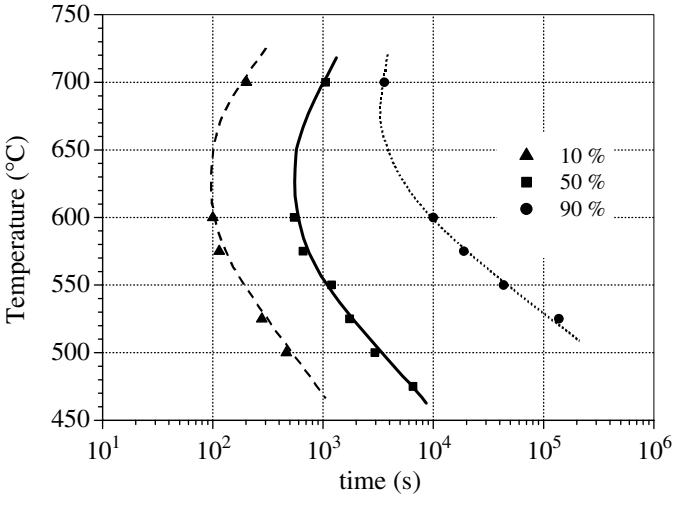

Figure 6. Time–Temperature-Transformation (TTT) diagram deduced from TEP measurements. The temperature where precipitation of copper in iron is fastest is around 650°C.

3.3. *TTT diagram*

The wide temperature range of TEP measurements presented in figure 3 and validated in the previous paragraph allows us to estimate the Time–temperature-transformation (TTT) diagram for the studied Fe–Cu model alloy. Figure 6 shows the temperature dependence of the time needed to achieve 10%, 50% and 90% of the precipitation reaction. This representation exhibits typical C-curves with a nose situated between 600 and 650°C. At these temperatures, reaction is almost complete in 10^4 s (3 h). This representation should be useful for optimization of precipitation hardening heat treatments involving copper precipitation and the general approach could be generalized to any kind of industrial alloy containing copper.

3.4. *Solubility limit: results and discussion*

In this section, solubility limits measured using the TAP and TEP are presented and compared. Apparent copper solubility limit can be deduced from TEP measurements: it is given by the solute content for the longest ageing time at each temperature using equation (7). Results are summarized in table 2 and presented in figure 7. Furthermore, TAP measurement of the copper solubility in the Fe–1.4 wt% Cu alloy annealed at 500°C has been found to be 0.17 ± 0.06 wt%.

The temperature range (500–700°C) of the present investigation is too wide to describe the solubility limit with the classical $\log_{10}[\mathrm{Cu}] = -A/T + B$, where T is expressed in Kelvin. Thus, a third term in T^2 has been added leading to $\log_{10}[\mathrm{Cu}]_{\mathrm{wt\%}} = -A/T^2 + B/T + C$. This expression has no simple physical meaning, but can be fitted to experimental data and describe all experimental points, including TAP measurements. It gives the following evolution of the apparent copper solubility limit:

$$\log_{10}[\mathrm{Cu}]_{\mathrm{wt\%}} = \frac{6111850}{T^2} - \frac{16478.2}{T} + 10.3242. \tag{8}$$

Table 2. Solubility limits of copper in iron corrected by the Gibbs–Thomson factor.

Temperature (°C)	450	475	500	525	550	575	600	700
Longest ageing time (s)			4×10^6	2.2×10^6	7.4×10^5	7.4×10^5	5×10^6	5.8×10^5
$S_{t\to\infty}$ (μV/K)			−1.486	−1.616	−1.759	−2.109	−2.419	−5.046
[Cu] (wt%)			0.172	0.188	0.206	0.252	0.293	0.698
R (nm)	–	–	15	–	–	–	55	70
[Cu] GT (wt%)	–	–	0.162	–	–	–	0.289	0.691

The Gibbs–Thomson effect decreases the solubility limit by 5%.

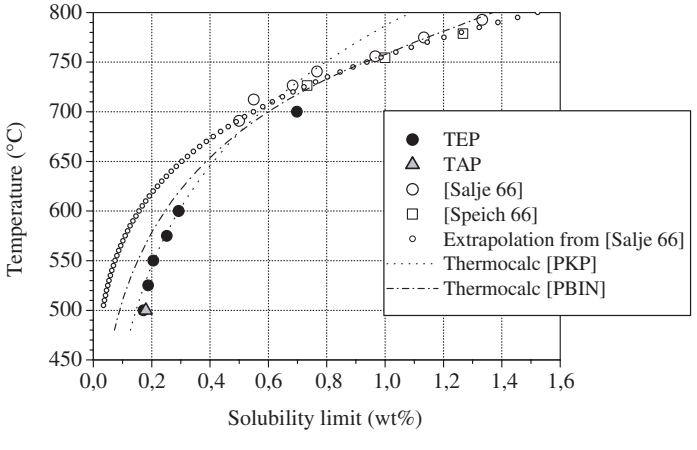

Figure 7. Solubility limit of copper in iron deduced from TEP measurement and corrected from the Gibbs–Thomson effect using the results of the SAXS measurements. The TAP gives a value in good agreement with the two other techniques, but much higher than extrapolation of the literature.

The second part of table 2 quantifies the effect of precipitate radius on copper solubility (i.e. the Gibbs–Thomson effect), for three temperatures. The precipitate size has been extrapolated at longest TEP measurement times using the LSW behaviour presented in figure 4, and then used to correct solubility measurements using the Gibbs–Thomson equation:

$$[\mathrm{Cu}]^{\mathrm{GT}}_{\mathrm{wt\%}} = [\mathrm{Cu}]_{\mathrm{wt\%}} \exp\left[-\frac{R_0}{R}\right] \text{ with } R_0 = \frac{2\gamma v_{\mathrm{at}}}{kT}, \tag{9}$$

where $\gamma = 0.4 \pm 0.1\ \mathrm{J/m^2}$ is the assumed interfacial energy of the precipitates [9] and $v_{\mathrm{at}} = 1.18 \times 10^{-29}\ \mathrm{m^3}$ is their atomic volume . This corrected solubility can be fitted by another set of parameters which gives the true equilibrium copper solubility limit in iron in the range 500–700°C:

$$\log_{10}[\mathrm{Cu}]^{\mathrm{GT}}_{\mathrm{wt\%}} = \frac{5771323}{T^2} - \frac{15763.84}{T} + 9.944961. \tag{10}$$

This second expression takes into account the fact that TEP measurements are made on a precipitate population with finite radius, and thus need to be corrected to give the solubility in equilibrium with precipitates of infinite size.

Figure 7 shows the experimental solubility limit evaluated from TEP measurements and compares it with the extrapolated solubility taken from literature [15] and solubility given by Thermocalc© software (thermodynamics calculation software: www.thermocalc.com) with two different databases. The TAP measurement performed at 500°C is also reported on this figure. TEP and TAP results are in very good agreement.

TEP measurements detect a higher solubility limit than the one expected by some results of the literature. This discrepancy has already been observed [32] but, to our knowledge, it has never been clearly explained. Actually, most of the solubility limits found in the literature come from extrapolation to low temperature of the measurements of Salje *et al*. [15] or Speich *et al*. [33] that were performed at temperatures higher than 700°C. The complex behaviour of the iron matrix in the temperature range (500–700°C) could certainly explain this discrepancy between extrapolated and measured values of solubility limit.

Measurement by SAXS of precipitate sizes allows a correction in the solubility limit (relative difference of 6% at 500°C and 1% at 700°C). Table 2 shows that the Gibbs–Thomson effect has an influence on the measurement of copper solubility, especially at low temperatures. This correction will be useful to make accurate model calibration because solubility limit has a very strong effect on modelled precipitation kinetics.

4. Conclusions

The solubility limit of copper has been investigated by studying copper precipitation kinetics in a wide temperature range. Three experimental devices have been used: (1) TEP to evaluate the copper content of the solid solution at the end of copper precipitation; (2) SAXS to measure precipitate sizes and thus take into account

the Gibbs–Thomson effect on copper solubility limit; (3) TAP to check locally the copper content of the solid solution. These three experimental techniques are in very good agreement, giving access to a precise and quantitative knowledge of copper precipitation kinetics and copper solubility limit in the range 500–700°C.

To study precipitates particles, SAXS has to be preferred (it gives access directly to the mean radius evolution), whereas copper solubility can be described more directly by TEP and TAP measurements.

The measured solubility limit of copper is significantly higher than the usual values found in the literature. However, the present measurements are the first direct measurements in a pure Fe–Cu alloy in this temperature range. In addition, a TTT diagram in the temperature range 475–700°C has been obtained.

These results can serve as the basis for modelling copper precipitation in iron at any scale: from the atomic scale where solubility is needed to validate inter atomic potentials, to classical thermodynamic modelling where the solubility limit is a key parameter driving the kinetics of precipitation. This last point will be detailed in a forthcoming paper.

Acknowledgements

Some of the authors are involved in a French scientific program called 'CPR Precipitation', in collaboration with Arcelor, Pechiney, CNRS, CEA, INPG, INSA Lyon, Université de Rouen, Université Aix-Marseille 3. Arcelor Research and Lucchini are acknowledged for financial support. F. Bley as well as the whole D2AM-ESRF team are gratefully acknowledged for their help with the SAXS experiments and data interpretation. V. Schmitt, A. Vincent and J. Merlin are acknowledged for helpful discussions.

References

[1] S.-J. Kim, C.G. Lee, T.H. Lee, *et al.*, ISIJ Int. **42** 1452 (2002).
[2] S.S.G. Banadkouki, D.Y. Yu and D.P. Dunne, ISIJ Int. **36** 61 (1996).
[3] S.I. Golubov, Y.N. Osetsky, A. Serrz, *et al.*, J. Nucl. Mater. **226** 252 (1995).
[4] S. Miloudi, S. Jumel, P. Pareige, *et al.*, in *Effects of Radiation on Materials: 19th Symposium* (ASTM, 1999), p. 1366.
[5] D.T. Llewellyn, Ironmaking Steelmaking **22** 25 (1995).
[6] M. Charleux, F. Liret, F. Bley, *et al.*, Phil. Mag. A **73** 883 (1996).
[7] P.J. Othen, H.L. Jenkins, G.D.W. Smith, *et al.*, Phil. Mag. Lett. **64** 383 (1991).
[8] S. Pizzini, K.J. Roberts and W.J. Phythian, Phil. Mag. Lett. **61** 223 (1990).
[9] M. Gouné, P. Mangis, E. Pinto de Costa, *et al.*, Rev. Métall. **1** 71 (2004).
[10] A. Deschamps, M. Militzer and W. Poole, ISIJ Int. **41** 196 (2001).
[11] A. Deschamps, M. Militzer and W.J. Poole, ISIJ Int. **43** 1826 (2003).
[12] F. Perrard, Caractérisation et modélisation de la précipitation du carbure de niobium et du cuivre dans les aciers bas carbone. Ph.D. thesis, Institut National Polytechnique de Grenoble (2004).
[13] Y. Le Bouar and F. Soisson, Phys. Rev. B **65** 094103–15 (2002).
[14] S. Schaumader and P. Binkele, Comput. Mater. Sci. **24** 42 (2002).
[15] G. Salje and M. Feller-Kniepmeier, J. Appl. Phys. **48** 1833 (1977).
[16] M.-H. Mathon, F. Maurry, A. Barbu, *et al.*, J. Phys. (Paris) **4** 193 (1994).
[17] M. Perez, Scripta Mater. **52** 709 (2005).

[18] F.J. Blatt, P.A. Shroeder, C.L. Fsiles, *et al.*, *Thermoelectric Power of Metals* (Plenum Press, New York and London, 1976).
[19] L. Nordheim and C.J. Gorter, Physica **2** 383 (1935).
[20] J.M. Pelletier, G. Vigier, J. Merlin, *et al.*, Acta Metall. **32** 1069 (1984).
[21] G.M. Raynaud and P. Guyot, Acta Metall. **36** 143 (1988).
[22] O. Glatter and O. Kratky (Editors), *Small Angle X-ray scattering* (Academic Press, London, 1982).
[23] T.P. Russell, J.S. Lin, S. Spooner, *et al.*, J. Appl. Cryst. **21** 629 (1988).
[24] A. Deschamps, M. Nicolas, F. Perrard, *et al.*, Rev. Métall. **5** 361 (2004).
[25] D. Blavette, A. Bostel, J.M. Sarrau, *et al.*, Nature **363** 432 (1993).
[26] P. Pareige, P. Auger, P. Bas, *et al.*, Scripta Metall. Mater. **33** 1033 (1995).
[27] M.K. Miller, A. Cerez, H.G. Hetherington, *et al.*, *Atom Probe Field Ion Microscopy* (Oxford University Press, Oxford, 1996).
[28] Y. Meyzaud and P. Parnière, Mém. Sci. Rev. Met. **71** 415 (1974).
[29] C. Wagner, Z. Elektrochem. **65** 581 (1961).
[30] I.M. Lifshitz and V.V. Slyozov, J. Phys. Chem. Solids **19** 35 (1961).
[31] R. Monzen, K. Takada and C. Watanabe, ISIJ Int. **44** 442 (2004).
[32] M.-H. Mathon, Etude de la precipitation et des mécanismes microscopiques de durcissement sous irradiation dans des alliages ferritiques dilués. Thesis, Paris XI (1995).
[33] G.R. Speich, J.A. Gula and R.M. Fisher, in *Electron Microprobe*, edited by T.D. McKinley, K.J. Heinrich and D.B. Witty (Wiley, New York, 1966), p. 525.